Energy Development and Technology 012

"Model Studies of Pore Stability and Evolution in Thermal Barrier Coatings (TBCs)"

A. M. Glaeser
University of California, Berkeley

January 2008

This paper is part of the University of California Energy Institute's (UCEI) Energy Development and Technology Working Paper Series. UCEI is a multi-campus research unit of the University of California located on the Berkeley campus.

UC Energy Institute
2547 Channing Way
Berkeley, California 94720-5180
www.ucei.org

This report is issued in order to disseminate results of and information about energy research at the University of California campuses. Any conclusions or opinions expressed are those of the authors and not necessarily those of the Regents of the University of California, the University of California Energy Institute or the sponsors of the research. Readers with further interest in or questions about the subject matter of the report are encouraged to contact the authors directly.

Working Paper Prepared for:
The University of California Energy Institute

Model Studies of Pore Stability and Evolution in Thermal Barrier Coatings (TBCs)

A. M. Glaeser
Department of Materials Science and Engineering
University of California
Berkeley, California 94720

☎: (510)-486-7262
fax: (510)-643-5792
Internet: *aglaeser@sapphire.berkeley.edu*

Funding Period: 7/1/06 to 6/30/07
Account: 07427-23845 (EE0701)

Summary:

Studies of the high-temperature morphological evolution of controlled-geometry surface cavities and of controlled-geometry internalized pores etched into the (100) and (111) surfaces of yttria-stabilized zirconia (YSZ) have been conducted. Results show significant crystallography-dependent variations in the morphologies and evolution rates. The terrace-ledge structures on (100) and (111) YSZ surfaces differ substantially. Internalized pores that are largely or partially bounded by {111} surfaces are particularly stabilized with regard to shape relaxation and axial instability. The results suggest that controlled variation of thermal barrier coating (TBC) texture and microstructure could result in significant changes in stability and lifetimes.

Introduction

During the period from July 1st, 2006 to June 30th, 2007 (and beyond) fundamental model studies of the evolution of the pore structure in thermal barrier coating (TBC) materials were conducted. TBCs are used extensively on air-cooled metallic components in the hot sections of engines and power-generation systems to provide thermal insulation and protect temperature-sensitive components from hot engine gases. TBCs permit higher operating temperatures and the associated higher thermal efficiencies result in substantial fuel savings and more efficient power generation.

The thermal conductivity, *k*, of a TBC is a critical materials parameter. As *k* decreases, further increases in operating temperature and thermal efficiency are possible. Voids in a TBC decrease *k* by an amount that is sensitive to the volume fraction, geometry and spatial arrangement of the voids; mechanical properties of the TBCs are also affected by the same factors. Voids can exist as equiaxed or elongated pores, and as cracklike defects. Time-dependent changes in the size, shape, and spatial distribution of pores and cracks can lead to significant changes in *k*, and a loss of insulating capability; concurrently, the strain tolerance of the coating can also decrease.

The work was motivated by the desire to establish a robust experimental framework for direct, quantitative assessment of pore and crack morphology evolution in TBCs. Information gained from such experiments would provide benchmark data for existing state-of-the-art yttria-stabilized zirconia (YSZ) TBCs, and allow exploration of other material systems that are candidates for future use as TBCs. Fundamental studies provide the information needed to design TBCs that can operate at even higher temperatures for longer periods than YSZ TBCs. Although YSZ TBCs have been in use in commercial aircraft for many years, a fundamental understanding of the factors that control the rate at which porosity undergoes morphological change and is removed during use is missing. Insights gained from model studies could potentially reveal processing modifications that would enhance the stability of currently used materials, providing short-term benefits while new TBC systems are developed.

Prior model studies of pore stability in aluminum oxide (alumina) ceramics have revealed that the crystallographic orientation of surfaces has a very profound effect on the evolution rate. Geometrically identical but crystallographically distinct pores can evolve at rates that differ by several orders of magnitude. To explore and assess such effects in TBC materials, the work focused on the most widely used base material for TBCs, YSZ. Photolithography and ion-beam etching were applied to optically transparent single-crystal YSZ substrates of two distinct surface orientations to produce controlled-geometry surface cavities. Solid-state diffusion bonding conditions were ultimately identified that successfully bonded etched/patterned YSZ substrates to unetched YSZ substrates to internalize the surface cavities, and simulate void structures in commercially produced TBCs. Both etched substrates and bonded substrate pairs were annealed at elevated temperatures, and the evolution of both surface cavities and internal pore structures were tracked using atomic force microscopy (AFM) for surface features, and a combination of light-optical and scanning-electron microscopies for internal and re-exposed features, respectively. The fabrication approach allows precise control over substrate surface crystallography, initial pore geometry, substrate-substrate misorientation, anneal time, and anneal temperature, allowing systematic examination of the microstructural and crystallographic variables that affect pore stability and evolution. The results of our UCEI-funded work establish that the techniques previously used for single-crystal aluminum oxide (sapphire) can be applied to YSZ, and there are indications that crystallographic texturing is one viable route to producing TBCs with increased use temperature, or longer lifetimes, or both.

Background

Ceramic thermal barrier coatings (TBCs) on air-cooled metallic components in the hot sections of engines and power-generation systems provide thermal insulation and protect these temperature-sensitive components from hot engine gases [1-5]. The use of TBCs in engines and turbines permits higher operating temperatures than would be possible without TBCs; the higher thermal efficiency results in substantial energy savings. Higher operating temperatures can also promote more complete combustion of conventional and alternative fuels, decrease the emission of oxides of nitrogen (NO_x) and particulate matter, and thus impart additional economic and environmental benefits. In a review of DOE's Advanced Turbine Systems Research Program, a National Academy of Science publication [6] estimated that developments stemming from DOE's sponsored research would result in domestic energy savings of $390 million for the period 2000–2005, and an additional $9.6 billion during the period 2006–2010, while reducing domestic NO_x emissions by 9793 and 211,000 tons during the 2000–2005 and 2006–2010 intervals, respectively. More widespread use of higher-efficiency, longer-lifetime TBCs in both the transportation (*e.g.*, aerospace, automotive) and electric-power-generation sectors would reduce the amount of petroleum, natural gas, and coal required to meet projected energy demand and have positive environmental impacts as well.

The thermal conductivity, *k*, of the TBC is a critical parameter [4, 5, 7-14]. If the steady-state heat flux through a TBC of fixed thickness is held constant, then as *k* decreases, the temperature drop from the TBC surface to the metal/TBC interface increases. If a maximum temperature for the metal is fixed by the desired system lifetime, decreasing *k* can allow an increase in the operating temperature and thermal efficiency.

The value of *k* is sensitive to the material selected for the TBC, and its microstructure. A range of ceramic materials has been explored for TBC use [5, 12-16]. A current mainstay is YSZ; a typical composition is 7 wt% Y_2O_3, 93 wt% ZrO_2. Compositional modifications, *e.g.*, low-level rare-earth-element additions to YSZ, can reduce *k* to 40% of the YSZ baseline [14, 16]. Internal voids in the form of pores or cracklike flaws are also effective in reducing *k*, and enhancing the insulating capability of the TBC. TBCs produced by air plasma spray (APS) methods [1, 5, 8, 15, 17], by electron beam physical vapor deposition (EB-PVD) [4, 5, 9-12, 18, 19], and by solution plasma spray (SPS) process [3] all contain micron-sized pores, and microcracks. Variations in the void volume fraction and pore geometry lead to variations in *k*. Other fabrication methods are under development with the goal of rapid and economic application of robust and stable low-*k* TBCs, and porosity is an essential microstructural component.

Ideally TBCs should function for long times (*e.g.*, >10,000 hours) at elevated temperatures (up to 1650°C in the future [14, 16]). Under these projected operating conditions, it is vital to understand time-dependent changes in the size, shape, and spatial distribution of pores and cracks at elevated temperature [1, 4, 5, 14, 16, 17]. Pores can disappear if the material densifies during high-temperature use, and the TBC literature describes this as a "sintering effect". Pores can also coarsen or change shape, and cracklike flaws can heal. Collectively, these changes can lead to significant time-dependent increases in *k*, and an associated loss of insulating capability. Thus, materials with promising as-fabricated properties may undergo serious degradation with time. Changes in the composition of a material that reduce *k* may also affect diffusion rates and reduce the rate at which pores evolve or disappear, or may change the rate-limiting process controlling pore evolution [20-23]. Alternatively, additives and dopants may enhance transport properties that lead to pore evolution [24]. The development of TBCs would thus benefit from an experimental method that allows direct observation and meaningful comparisons of pore stability and characterization of evolution behavior in candidate TBCs.

Research Overview

As-fabricated, porous polycrystalline TBCs are not optically transparent. As a result, monitoring pore evolution requires tedious experimental studies of 2-D cross sections, or indirect methods that provide only spatially averaged information (*e.g.*, density measurements and measurements of thermal conductivity) [14, 17]. Systematic study of well-defined flaws is not possible. The thrust of our effort was to develop an experimental method that would allow study of the evolution of, and interaction between artificially generated pores and flaws of controlled and reproducible geometry in TBCs at elevated temperature. Successful demonstration of such a method was viewed as key to successfully developing external funding that would allow more detailed studies of approaches for stabilizing pores and cracklike flaws in low-*k*, high-temperature TBCs.

A two-pronged effort was made. Since pore shape changes and pore disappearance both require the movement of surfaces, experiments were conducted in which shallow controlled-geometry cavities were introduced into single-crystal YSZ surfaces of different crystallographic character, and their morphological evolution was followed. The hope was to obtain indications of surface stability, a factor that greatly influences the energetics and kinetics of surface migration. In parallel, efforts were made to develop bonding techniques to encapsulate or internalize lithographically generated surface cavities, thereby converting them into internal pores whose shape and crystallography could be controlled and varied. This proved to be very challenging, but was ultimately achieved.

The results of these two research thrusts show that very different surface topographies develop when the crystallographic character of the YSZ surface is changed. There are suggestions that this will lead to different rates of surface profile relaxation, and these differences should translate into differences in the rates at which internalized pores bounded by such surfaces migrate. This in turn suggests that differing rates of pore shape change and pore disappearance can be developed in a material of fixed chemistry by varying the crystallographic texture of coatings, and thus, the orientation of the surfaces. Studies of the relaxation of internalized high-aspect-ratio pore channels confirm that changes in the channel axis orientation, which alters the nature of the bounding surfaces, can have a significant impact on rate at which the pores reach an equilibrium geometry. Details of this work are summarized in the Research Results section.

Research Results

Preparation of Model Surface and Pore Structures

All samples used in this research were YSZ single crystals, containing 9.5mol% Y_2O_3 and acquired from CrysTec GmbH in Berlin, Germany. The crystals were received as 10 mm × 10 mm substrates, with both faces polished, and with faces parallel to one of the following six crystallographic planes: (100), (110), (111), (211), (311), and 5° off of (100). Sample thickness varied from 0.5 mm to 1.0 mm. Orientations of samples used were confirmed with Laue backscatter diffraction.

Experiments performed included analysis of morphological changes after annealing at temperatures ranging from 1000° to 1800°C of the following types of surfaces: polished flat surfaces, lithographed surfaces, internal crack-like voids, and internal channel-shaped voids. All samples except for the first group of flat surfaces were ion-beam etched. Lithography was done in a class 100 clean room. Samples were cleaned by ultrasonication for 15 min each in SC-1 (5:1:1 of H_2O:H_2O_2:NH_4OH) and SC-2 (6:1:1 of

H_2O:H_2O_2:HCl) and then were baked out in a box furnace at 120°C just prior to lithography. Microposit™ S1818™ photoresist was then spun onto samples at 5500 rpm on a Headway spinner. The photoresist was selectively exposed to UV light in a 4× -reduction Canon FPA-141 Fine Pattern Projection Aligner using chrome-coated glass masks with arrays of digitally created geometric features. After chemically dissolving the exposed regions of photoresist, these features were etched into the substrate surfaces with neutralized argon ions in a Veeco Ionmill. After removing the residual photoresist, etch depths were measured with both a profilometer and an AFM.

For samples that were diffusion bonded, they were again cleaned with SC-1 and SC-2 and then bonded in a tantalum-element vacuum hot press with alumina furniture. Bonding conditions were varied initially in an attempt to idealize the process. The final samples made, 111C-BMP and 100C-BMP, were bonded at 1100°C with a load of 18.5 MPa. These conditions led to reliable bonds, however some sample cracking still occurred. With the exception of sample 100A-BMP, which was annealed in a tungsten-element vacuum furnace at 1700° and 1800°C, all samples were annealed in the range of 1000° to 1600°C in a molybdenum-disilicide-element air furnace in a covered alumina crucible. Anneal times ranged from 2 h to 256 h with ramp rates constant at ±300°C/h.

The first two groups of experiments involved examination of morphological changes of exterior surface features. The flat surfaces examined were as-polished samples, aligned with one of the six crystallographic planes mentioned above. The samples created for this portion of the research are listed in the first section of Table 1, and are referred to as the unetched surface topography (UST) samples. The second group of experiments, referred to as the surface topography of lithographed square arrays (STL) samples in Table 1, included samples that had specific features lithographically etched onto their surfaces. Examples of one set of arrays of pits etched on the surface are included in Figure 1. Two other sizes of features were also used. These features created a wide range of initial non-equilibrium shaped surfaces whose morphological evolution during anneals could be tracked and quantified. In two cases, pairs of samples with two different orientations, (100) and (111), were created and annealed concurrently so that all other variables were kept the same. This allowed a direct assessment of surface-orientation-based differences in evolution. Between anneals surface features from all of these samples were examined with a Molecular Imaging PicoSPM II AFM with a silicon nitride tip in contact mode.

The second two groups of experiments involved the examination of internal voids in bonded pairs of YSZ. Samples listed in the third section of Table 1, bonded lithographed matched pairs (BMP), were used for both of these experiments. Controlled-geometry features of both crack-like shapes and channel-like shapes were lithographically etched onto surfaces of both (100) and (111) faces of YSZ. Examples of the high aspect ratio channel-like features that are rotated every 15° to sample a variety of crystallographic directions are shown in Figure 2. Etched surfaces were internalized by diffusion bonding the etched faces to non-etched faces of like-orientation, simulating internal pores in a continuous single crystal. Feature shapes were documented *via* optical microscopy, through the transparent sample, in between each anneal so that evolution could be monitored and measured. Figure 3a shows an SEM image of etched features on the sample surface and Figure 3b shows an optical image of internal void features after bonding. Samples 100A-BMP and 100B-BMP were also cut open after anneals, polished, and imaged *via* SEM to examine the cross-section of internal features.

Table 1. List of samples created with their respective heat treatments

	Unetched Surface Topography (UST)							
Sample Name	A-UST	1 A-UST	2A-UST	3A-UST	4A-UST	5A-UST	6A-UST	7A-UST
Orientation/ Heat Treatment	(100)/ None	(100)/ 32h @ 1000°C	(100)/ 32h @ 1100°C	(100)/ 32h @ 1200°C	(100)/ 32h @ 1300°C	(100)/ 32h @ 1400°C	(100)/ 32h @ 1500°C	(100)/ 32h @ 1600°C
Sample Name	0B-UST	1B-UST	2B-UST	3B-UST	4B-UST	5B-UST	6B-UST	7B-UST
Orientation/ Heat Treatment	(5°off 100)/ None	(5°off 100)/ 32h @ 1000°C	(5°off 100)/ 32h @ 1100°C	(5°off 100)/ 32h @ 1200°C	(5°off 100)/ 32h @ 1300°C	(5°off 100)/ 32h @ 1400°C	(5°off 100)/ 32h @ 1500°C	(5°off 100)/ 32h @ 1600°C
Sample Name	0C-UST	1C-UST	2C-UST	3C-UST	4C-UST	5C-UST	6C-UST	7C-UST
Orientation/ Heat Treatment	(110)/ None	(110)/ 32h @ 1000°C	(110)/ 32h @ 1100°C	(110)/ 32h @ 1200°C	(110)/ 32h @ 1300°C	(110)/ 32h @ 1400°C	(110)/ 32h @ 1500°C	(110)/ 32h @ 1600°C
Sample Name	0D-UST	1D-UST	2D-UST	3D-UST	4D-UST	5D-UST	6D-UST	7D-UST
Orientation/ Heat Treatment	(111) /None	(111)/ 32h @ 1000°C	(111)/ 32h @ 1100°C	(111)/ 32h @ 1200°C	(111)/ 32h @ 1300°C	(111)/ 32h @ 1400°C	(111)/ 32h @ 1500°C	(111)/ 32h @ 1600°C
Sample Name	0E-UST	1E-UST	2E-UST	3E-UST	4E-UST	5E-UST	6E-UST	7E-UST
Orientation/ Heat Treatment	(211)/ None	(211)/ 32h @ 1000°C	(211)/ 32h @ 1100°C	(211)/ 32h @ 1200°C	(211)/ 32h @ 1300°C	(211)/ 32h @ 1400°C	(211)/ 32h @ 1500°C	(211)/ 32h @ 1600°C
Sample Name	0F-UST	1F-UST	2F-UST	3F-UST	4F-UST	5F-UST	6F-UST	7F-UST
Orientation/ Heat Treatment	(311)/ None	(311)/ 32h @ 1000°C	(311)/ 32h @ 1100°C	(311)/ 32h @ 1200°C	(311)/ 32h @ 1300°C	(311)/ 32h @ 1400°C	(311)/ 32h @ 1500°C	(311)/ 32h @ 1600°C

	Surface Topography of Lithographed Square Arrays (STL)				
Sample Names (annealing pair)	100A-STL (100 orientation) and 111A-STL (111 orientation)				
Total Anneal Times	0h	2h @ 1000°C	8h @ 1000°C		
Sample Names (annealing pair)	100B-STL (100 orientation) and 111B-STL (111 orientation)				
Total Anneal Times	0h	2h @ 1200°C	8h @ 200°C	32h @ 1200°C	128h @ 1200°C
Sample Name	100e-STL (100 orientation)				
Total Anneal Times	0h	2h @ 1600°C	8h @ 1600°C	32h @1600°C	128h @ 1600°C
	Bonded Lithographed Matched Pairs (BMP)				
Sample Name	100A-BMP				
Description	(100) Matched pair with mixed large geometric shapes lithographed and internalized, used for initial crack healing experiment, anneal temperature determination, and cross-sectioning methodology. This sample was annealed in a vacuum environment (~10^{-5} torr)				
Heat Treatment	0h	19h @ 1700°C	19h @ 1700°C + 18h @ 1800°C		
Sample Name	100B-BMP				
Description	(100) Matched pair with "starburst" features (long channels and wide cracks) lithographed and internalized, used for preliminary gauging of channel behavior relative to heat treatments and for examining cross-section of channels prior to breakup.				
Heat Treatment	0h	128h @ 1400°C	128h @ 1400°C + 1h @ 1600°C	128h @ 1400°C + 140+h @ 1600°C	
Sample Name	100C-BMP				
Description	(100) Matched pair with "starburst" features lithographed and internalized, always heat treated with sample 111C-BMP, used for comparison of crack healing and Rayleigh instability behavior between these two samples, in order to infer crystallography-based differences in morphological progression.				
Heat Treatment	0h	16h @ 1600°C	32h @ 1600°C	64h @ 1600°C	128h @ 1600°C	256h @ 1600°C
Sample Name	111C-BMP				
Description	(111) Matched pair with "starburst" features lithographed and internalized, always heat treated with sample 100C-BMP, used for comparison of crack healing and Rayleigh instability behavior between these two samples, in order to infer crystallography-based differences in morphological progression.				
Heat Treatment	0h	16h @ 1600°C	32h @ 1600°C	64h @ 1600°C	128h @ 1600°C	256h @ 1600°C

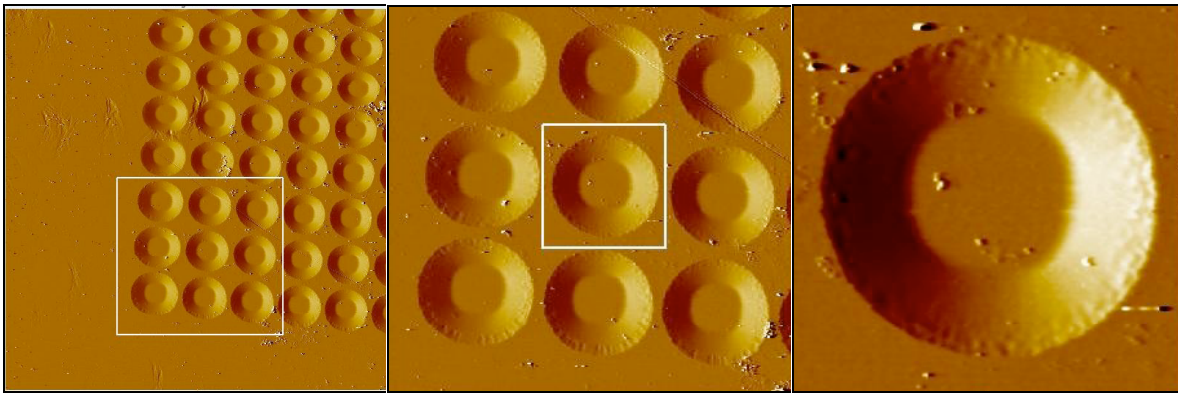

(a) (b) (c)

Figure 1. AFM scans of arrays of round features just etched on the YSZ surface. (a) is 80 μm × 80 μm, (b) is 35 μm × 35 μm, and (c) is 10.5 μm × 10.5 μm. The feature depth is ~250 nm.

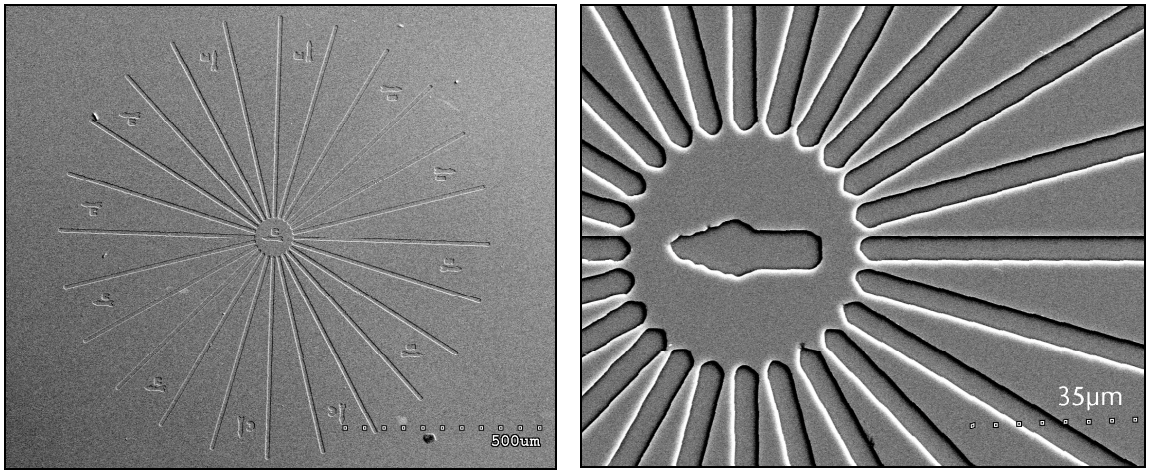

(a) (b)

Figure 2. SEM images of etched surface features (a) is an entire "starburst" feature and (b) is a close up of the center area of the starburst.

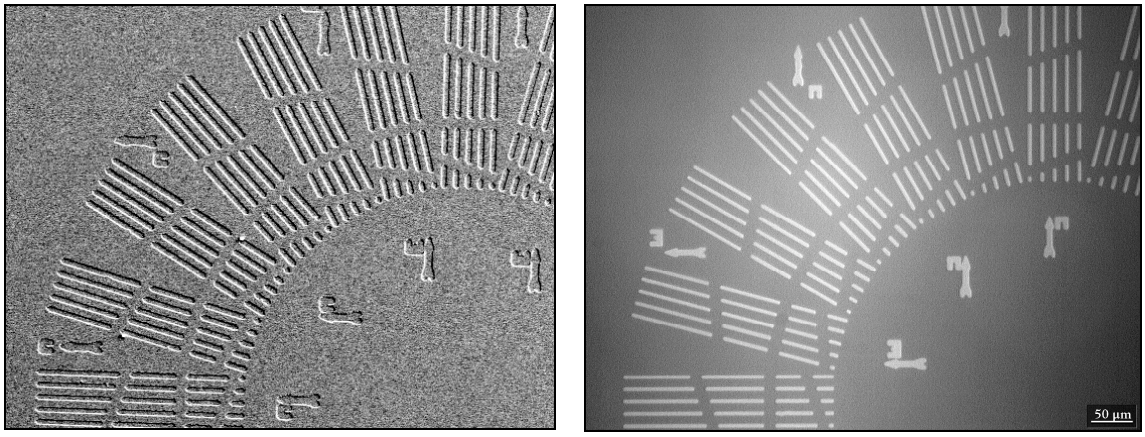

(a) (b)

Figure 3. Similar features viewed (a) by SEM on the surface after etching and (b) optically, in reflection mode, as internalized pores after bonding.

Model Studies of Surface Topography Evolution

At temperatures sufficiently high to activate diffusion, the topography of initially flat single crystal surfaces can evolve in one of three distinct ways; they can develop terrace-ledge type surfaces, they can develop hill-and-valley type surfaces, or they can remain flat. Either of the first two paths indicates anisotropic surface energies. Since surface energy anisotropy has been shown to be a stabilizing factor in sapphire, the first set of experiments, the Unetched Surface Topography series, was done to determine whether the surfaces of YSZ also exhibited anisotropic surface energy at temperatures from 1000°C to 1600°C. The flat surfaces examined were on as-polished samples, aligned with one of the six crystallographic planes mentioned previously.

Samples were annealed at temperatures of 1000°C to 1600°C with 100°C increments in the annealing temperature. Surfaces of all available initially flat and polished samples became stepped after heat-treating at all temperatures within this range. Examples of three of the (111) surfaces are given in Figure 4. Since initial surfaces were within 1° of their nominal orientations, steps created due to slight miscuts were expected and account for the stepping seen in all samples. The terraces are flat and parallel and the ledges are significantly shallower than wide. For example, at 1300°C, the steps are ~200 nm wide and ~0.5 nm in height. This corresponds to a miscut of 0.14°. The existence of steps is thus attributed to faceting due to a slightly miscut surface rather than the creation of hill-and-valley structures. This indicates that the (111) surface is stable, but surfaces at a slight angle from it will form (111) terraces with inclined steps at all temperatures sampled. The (100) surface also was stepped. As the miscut increases, the terrace width decreases, and the step/ledge density increases. A surface that was initially 5° off of (100) developed a faceted surface with the larger facet very close to 5° from the original surface, indicating that the (100) surface is more stable than a surface cut 5° from the (100), as expected.

The second set of surface samples, the Surface Topography of Lithographed Square Arrays (STL) series, which were first etched with arrays of pits as shown in Figure 1, were also created to determine whether morphological differences exist after annealing features of the same initial shape on different crystallographic surfaces. For these features, the average angle of inclination at the side of the etched feature, relative to the original surface is approximately 3°. As can be clearly seen in Figure 5, there are distinct differences in behavior between features on the (100) surface and the (111) surface. The most obvious is that the (100) features have large steps that are more visible than the (111) steps at this scale. Step height averages 11 nm on the (100) sample, from the linescan shown in Figure 6, relative to an average 0.3 nm height of the resolvable steps on the (111) sample, which can be seen most clearly as thin lines in the top center of Figure 5b. The second noticeable difference between features on the two samples is that the (100) sample has a number of pits and bumps, while the (111) sample is very smooth. This is also illustrated in another pair of AFM images of similar features shown in Figure 7, and is consistent throughout both samples. The third noticeable difference, illustrated in Figure 8, is that step edges in the (100) sample waver and are not concentric while the steps in the (111) sample do not intersect.

All three of these differences suggest that mass transport is easier on or near the (100) surface than the (111) surface. The larger steps indicate more step coalescence has occurred and mass has traveled farther on the (100) surface than the (111), which is not coalescing or is coalescing at a slower rate. The pits and bumps on the (100) sample are evidence of easier nucleation of atomic-height patches or holes on that surface relative to the (111). These nucleation sites, which are necessary for transport and morphological changes, will be discussed again in the following section. The intertwining step edges may be part or all of the reason that the

(100) steps are interacting more rapidly than the (111) steps, and the lack of interacting steps on the (111) surface means that the path to step coalescence is more difficult. Taken together, these factors indicate that the (111) surface is more stable to morphological changes.

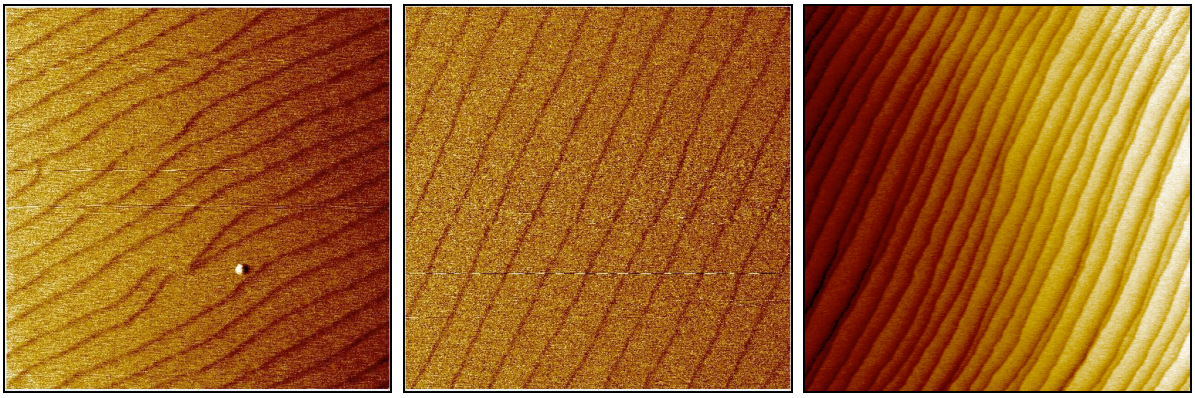

(a) (b) (c)

Figure 4. 5 μm × 5 μm AFM images of (111) samples annealed for 32 h at (a) 1100°C, (b) 1300°C, and (c) 1600°C

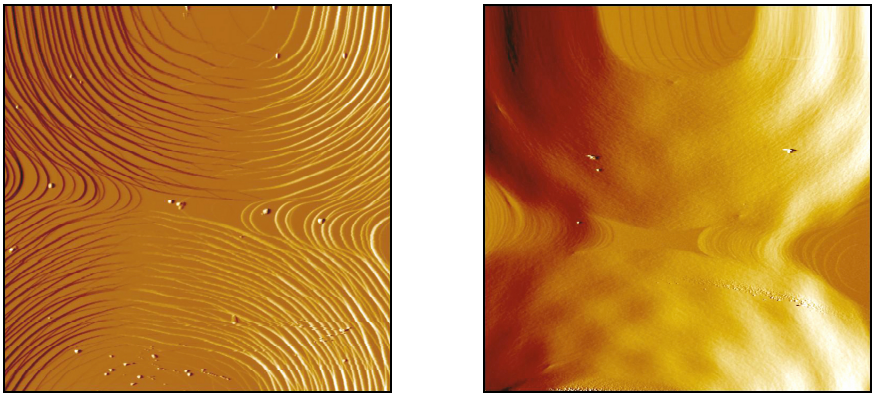

(a) (b)

Figure 5. 10 μm × 10 μm images of the same (large) feature annealed for 128 h hours in air at 1200°C on (a) the (100) surface and (b) the (111) surface of YSZ.

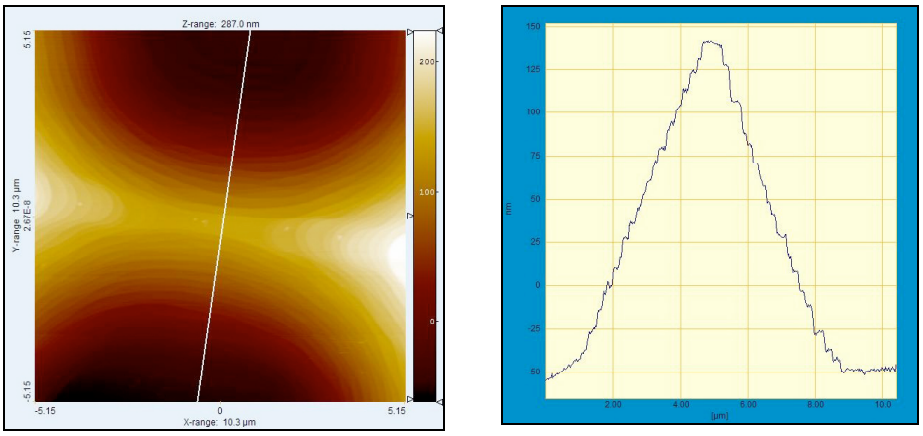

(a) (b)

Figure 6. AFM line scan of the (100) surface shown in Fig. 5a. (a) shows the topographical image with the line taken and (b) is the resulting depth profile of the linescan, which is approx. 10 µm long, and the height varies approx. 200 nm from ridge to valley.

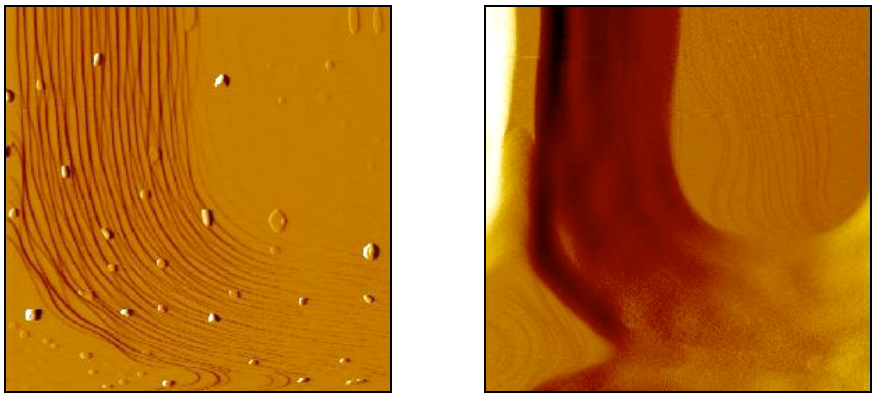

(a) (b)

Figure 7. 10 µm × 10 µm images of the same feature annealed for 128 h hours in air at 1200°C on (a) the (100) surface and (b) the (111) surface of YSZ.

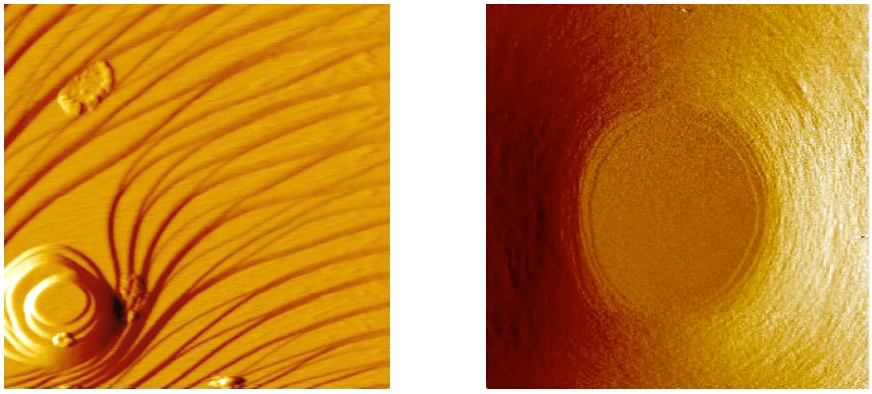

(a) (b)

Figure 8. 3 µm × 3 µm images of the feature annealed for 128 h hours in air at 1200°C on (a) the (100) surface and (b) the (111) surface of YSZ.

Model Studies of Pore-Channel Evolution

High-aspect-ratio phases such as rods, fibers, and wires are prone to axial instabilities that disrupt the continuous phase and convert it into a string of isolated features with some characteristic spacing. This arises because the rod has a high surface-to-volume ratio, and shape changes can lower the total surface energy. The process leading to breakup involves a progressive increase in the amplitude of a periodic axial perturbation in the rod or fiber radius. The earliest assessments of this process, by Plateau [25] and Rayleigh [26] in the 1800s treated a sinusoidal wave acting on a fluid in which the surface energy is independent of the surface orientation. The analyses for fluids yield a minimum wavelength, λ_{min}, that must be exceeded if amplitude growth is to lower the total surface energy. Plateau was the first to show that $\lambda_{min} = 2\pi R$. Rayleigh showed that for inviscid liquids the growth rate varied with wavelength λ, and that a specific wavelength, λ_{max}, was associated with the most rapid amplitude growth. The periodicity of breakup is thus expected to reflect the value of λ_{max}, which in the case of inviscid fluids is 9.02R.

Nearly 100 years later, Nichols and Mullins [27] extended the approach of Rayleigh to idealized solids with isotropic surface energy. The Nichols and Mullins result also applies to cylindrical pores in solid materials, and thus would pertain to pores in an idealized solid. For solids, the value of λ_{max} hinges on the dominant transport mechanism, and can vary from 8.89R to 13.02R. In crystalline materials, the surface energy γ will generally vary with surface orientation. Cahn [28] was the first to consider the effect of surface energy anisotropy on the energetics of Rayleigh instabilities, and showed that $\lambda_{min}^{anisotropic}$ could be increased or decreased relative to $2\pi R$ depending upon whether γ increased or decreased as the rod or pore surface was perturbed. Stolken and Glaeser [29, 30]analyzed the kinetics of surface-diffusion-controlled amplitude growth and showed that $\lambda_{max} = \sqrt{2}\lambda_{min}^{anisotropic}$, and that the time required for breakup scales with λ_{max}^2.

It follows that identifying orientations with large values of λ_{max} can profoundly increase stability and lifetimes. This is particularly relevant to pores in TBCs generated by e-beam physical vapor deposition (EB-PVD), which is used for high-performance applications. Introducing pore channels into (100) and (111) surfaces, and aligning the axes of the pores along a variety of directions is effective in identifying orientations that resist breakup. Since displacement of surfaces is also essential to pore disappearance, orientations that are stabilized to Rayleigh instabilities would also be expected to resist disappearance.

As described earlier, pore channels of controlled size (R ≈ 0.54 μm, length ≈ 155 μm) and crystallographic orientation were introduced into the (111) and (100) surfaces of YSZ by lithography, ion beam etching and diffusion bonding. Figure 9 shows a pore array after bonding but before annealing. Since the letters and arrows act as fiducial marks and allow each feature to be catalogued, and the optical transparency of YSZ allows nondestructive evaluation of the evolution of each internal feature, it becomes possible to reconstruct the temporal evolution. Figure 10 compares the behavior at 1600°C. Recalling that the channel cross-section is initially wide (3 μm) and shallow (0.3 μm), the differences in the behavior of (100) and (111) samples shows a clear effect of the dominant bounding plane on shape relaxation kinetics. The microstructures indicate that the (111) bounding surfaces are more difficult to displace, and this forestalls the development of a more equiaxed cross section. The higher magnification views show that after 256 h, selected channels in the (100) sample have broken up into shorter segments or into periodic arrays of pores. The (111) sample has undergone minimal change in morphology. Similar differences have been seen in sapphire, with the

slowest-moving planes being those for which dislocations normal to the plane have the largest Burgers vector. Dislocations can provide ledges that act as preferred sites for material removal or addition. In the absence of a source of ledges, movement of the surface can require the nucleation of an atomic height (or depth) patch on the migrating surface. This nucleation event is difficult, and the associated nucleation energy barrier can be sufficient to lock a surface, and thus the shape into a nonequilibrium configuration. Since the differences in the energies of stable surfaces tend to be less than a factor of two, it is unlikely that the driving force for evolution of the (100) and (111) samples larger than a factor of two. Since the evolution rate is proportional to the driving force for diffusion-controlled processes, it would be difficult to rationalize the observed behavioral differences as being the result of driving force differences. Instead the results suggest that for the more stable (111) samples, a nucleation energy barrier [31] may play a role, and the mechanisms of evolution of the (100) and (111) samples differ.

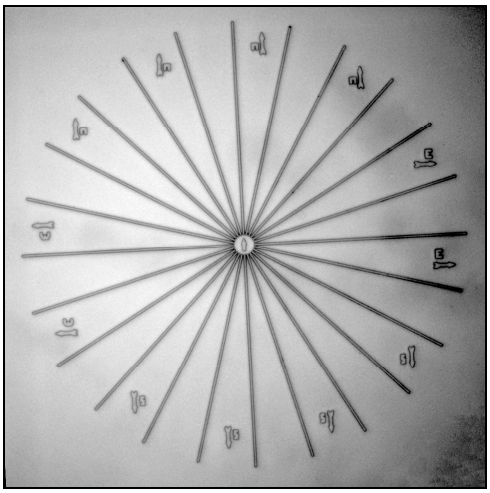

Figure 9. Optical image of channel starburst pattern internalized in a bonded pair of YSZ single crystals.

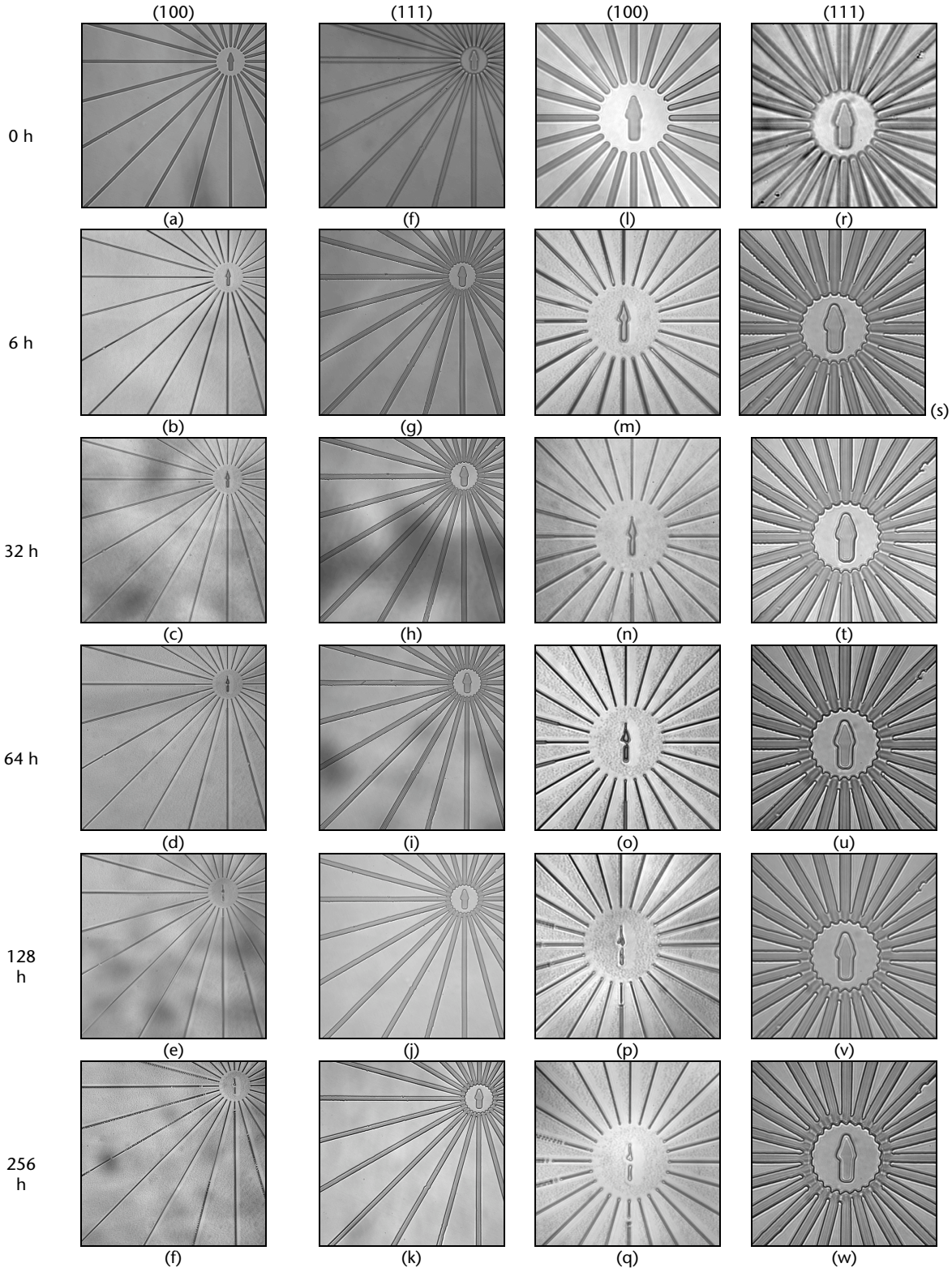

Figure 10. Progression of channel starburst features between anneals at 1600°C in air. The left column (a-f) is from the (100) sample and the next (g-k) is from the (111) sample. The next pair is the same regions, at higher magnification. The third column (l-q) is from the (100) sample, and the right most (r-w) is from the (111) sample.

Additional studies were performed on a second (100) sample to explore the orientation-dependent differences in stability. The sample was annealed in air for 128 h at 1400°C (with little obvious change of pore shape) and then for cumulative anneal times spanning 140 to 180 h at 1600°C. After 180 h, it appeared that channels oriented along $\langle 011 \rangle$ directions had enhanced stability, as seen in Figure 11. This sample was then cut perpendicular to the plane of the pore channels along a $\langle 100 \rangle$ direction. Figure 12 shows the cross sections of pore channels. Even after correcting for the elongation that occurs when the cut is not perpendicular to the axis of the channel, differences in the evolution rate and extent are evident. More detailed analysis of cross-sectional geometries has revealed that the stabilized channels oriented along $\langle 011 \rangle$ directions are partially bounded by {111} faces, which Figure 10 shows to have slow relaxation kinetics.

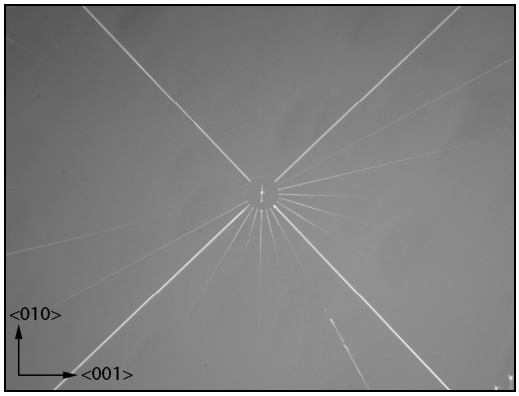

Figure 11. Reflection optical image of channel starburst pattern on the (100) plane after annealing and just prior to cross-sectioning.

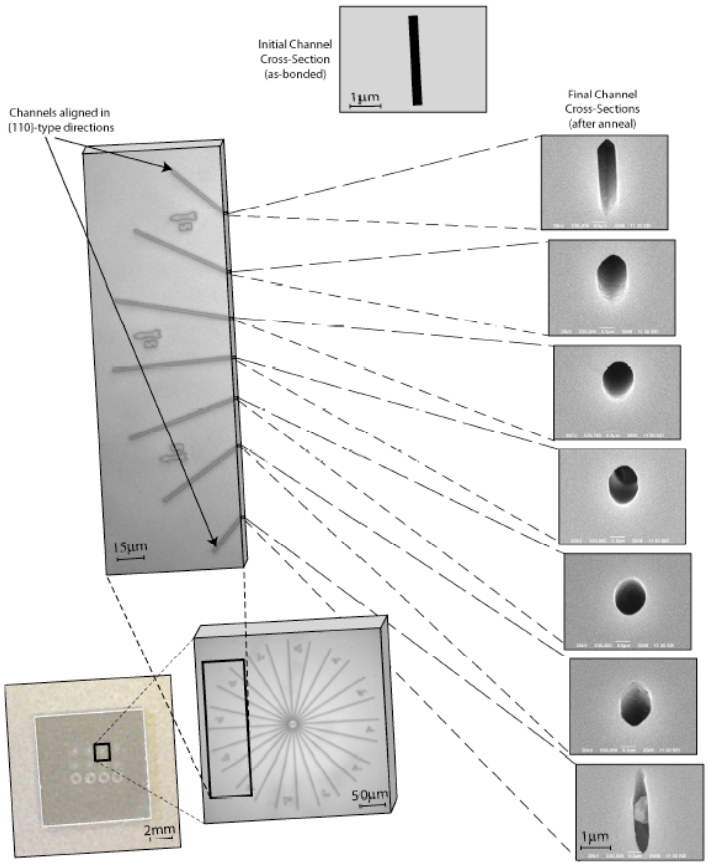

Figure 12. Cross-sectioned channels.

References:

1. B. Siebert, C. Funke, R. Vassen, and D. Stover, "Changes in porosity and Young's modulus due to sintering of plasma sprayed thermal barrier coatings," *Journal of Materials Processing Technology*, **92-93**, [30 Aug.], 217-23 (1999).
2. R. N. Katz, "Advanced Ceramics: Thermal Barrier Coatings Beat the Heat," http://www.ceramicindustry.com/CDA/ArticleInformation/features/BNP__Features__Item/0,2710,23950,00.html, (2001).
3. N. P. Padture, K. W. Schlichting, T. Bhatia, A. Ozturk, B. Cetegen, E. H. Jordan, M. Gell, S. Jiang, T. D. Xiao, P. R. Strutt, E. Garcia, P. Miranzo, and M. I. Osendi, "Towards durable thermal barrier coatings with novel microstructures deposited by solution-precursor plasma spray," *Acta Materialia*, **49**, [12], 2251-7 (2001).
4. J. R. Nicholls, K. J. Lawson, A. Johnstone, and D. S. Rickerby, "Methods to reduce the thermal conductivity of EB-PVD TBCs," *Surface & Coatings Technology*, **151**, 383-391 (2002).
5. D. R. Clarke and C. G. Levi, "Materials design for the next generation thermal barrier coatings," *Annual Review of Materials Research*, **33**, 383-417 (2003).
6. "Energy Research at DOE: Was it Worth It? Energy Efficiency and Fossil Energy Research 1978 to 2000," http://www.nap.edu/openbook/0309074487/html/126.html, (2001).

7. S. Raghavan, H. Wang, R. B. Dinwiddie, W. D. Porter, and M. J. Mayo, "The effect of grain size, porosity and yttria content on the thermal conductivity of nanocrystalline zirconia," *Scripta Materialia*, **39**, [8], 1119-1125 (1998).
8. R. W. Trice, Y. J. Su, K. T. Faber, H. Wang, and W. Porter, "The role of NZP additions in plasma-sprayed YSZ: microstructure, thermal conductivity and phase stability effects," *Materials Science and Engineering a-Structural Materials Properties Microstructure and Processing*, **272**, [2], 284-291 (1999).
9. S. Gu, T. J. Lu, D. D. Hass, and H. N. G. Wadley, "Thermal conductivity of zirconia coatings with zig-zag pore microstructures," *Acta Materialia*, **49**, [13], 2539-2547 (2001).
10. H. Guo, B. Xiaofang, G. Sheeengkai, and X. Huibin, "Microstructure Investigation on Gradient Porous Thermal Barrier Coating Prepared by EB-PVD," *Scripta Materialia*, **44**, [4], 683-687 (2001).
11. D. D. Hass, A. J. Slifka, and H. N. G. Wadley, "Low thermal conductivity vapor deposited zirconia microstructures," *Acta Materialia*, **49**, [6], 973-983 (2001).
12. K. Matsumoto, Y. Itoh, and T. Kameda, "EB-PVD process and thermal properties of hafnia-based thermal barrier coating," *Science and Technology of Advanced Materials*, **4**, [1-2], 153-158 (2003).
13. Y. J. Su, R. W. Trice, K. T. Faber, H. Wang, and W. D. Porter, "Thermal conductivity, phase stability, and oxidation resistance of Y3Al5O12 (YAG)/Y2O3-ZrO2 (YSZ) thermal-barrier coatings," *Oxidation of Metals*, **61**, [3-4], 253-271 (2004).
14. D. Zhu and R. A. Miller, "Thermal Conductivity of Advanced Ceramic Thermal Barrier Coatings Determined by a Steady-State Laser Heat-Flux Approach," *NASA/TM–2004-213040*, (2004).
15. M. B. Beardsley, P. G. Happoldt, K. C. Kelley, E. F. Rejda, and D. C. Socie, "Thermal Barrier Coatings for Low Emission, High Efficiency Diesel Engine Applications," Society of Automotive Engineers, Inc., Warrendale, PA 1999.
16. D. Zhu, S. R. Choi, and R. A. Miller, "Development and Fatigue Testing of Ceramic Thermal Barrier Coatings," *NASA/TM–2004-213083*, (2004).
17. G. Antou, G. Montavon, F. Hlawka, A. Cornet, and C. Coddet, "Characterizations of the pore-crack network architecture of thermal-sprayed coatings," *Materials Characterization*, **53**, 361-72 (2004).
18. Y.-C. Jung, T. Sasaki, T. Tomimatsu, K. Matsunaga, T. Yamamoto, Y. Kagawa, and Y. Ikuhara, "Distribution and structures of nanopores in YSZ-TBC deposited by EB-PVD," *Science and Technology of Advanced Materials*, **4**, [6], 571-74 (2003).
19. T. Kato, K. Matsumoto, H. Matsubara, Y. Ishiwata, H. Saka, T. Hirayama, and Y. Ikuhara, "Transmission electron microscopy characterization of a Yttria-stabilized zirconia coating fabricated by electron beam–physical vapor deposition," *Surface & Coatings Technology*, in press (2004).
20. M. Kitayama, T. Narushima, W. C. Carter, R. M. Cannon, and A. M. Glaeser, "The Wulff shape of alumina: I. Modeling the kinetics of morphological evolution," *J. Am. Ceram. Soc. (USA)*, **83**, [10], 2561-71 (2000).
21. M. Kitayama, T. Narushima, and A. M. Glaeser, "The Wulff shape of alumina. II. Experimental measurements of pore shape evolution rates," *J. Am. Ceram. Soc. (USA)*, **83**, [10], 2572-83 (2000).
22. M. Kitayama and A. M. Glaeser, "The Wulff shape of alumina. III. Undoped alumina," *J. Am. Ceram. Soc. (USA)*, **85**, [3], 611-22 (2002).

23. M. Kitayama and A. M. Glaeser, "The Wulff Shape of Alumina: IV. Ti(IV)-Doped Alumina," *J. Am. Ceram. Soc. (USA)*, (in press).
24. J. D. Powers and A. M. Glaeser, "Titanium Effects on Sintering and Grain Boundary Mobility of Alumina," *Ceram. Eng. Sci. Proc.*, **18**, [4], 617-23 (1997).
25. M. T. Plateau, "On the recent theories of the constitution of jets of liquid issuing from circular orifices," *Philosophical Magazine S4*, **12**, [79], 268-97 (1856).
26. Lord Rayleigh, "On the instability of jets," *Proceedings of the London Mathematical Society*, **10**, 4-13 (1879).
27. F. A. Nichols and W. W. Mullins, "Surface- (interface-) and volume-diffusion contributions to morphological changes driven by capillarity," *Transactions of the Metallurgical Society of AIME*, **233**, 1840-8 (1965).
28. J. W. Cahn, "Stability of rods with anisotropic surface free energies," *Scripta Metallurgica*, **13**, 1069-1071 (1979).
29. J. S. Stölken and A. M. Glaeser, "The morphological evolution of cylindrical rods with anisotropic surface free energy via surface diffusion," *Scripta Metallurgica et Materialia*, **27**, [4], 449-54 (1992).
30. A. M. Glaeser, "A new approach to investigating surface transport in ceramics," in *Mass and Charge Transport in Ceramics*, Vol. 71, K. Koumoto, L. M. Sheppard, and H. Matsubura, Eds. Westerville, OH: American Ceramic Society, 1996, pp. 117-136.
31. W. W. Mullins and G. S. Rohrer, "Nucleation barrier for volume-conserving shape changes of faceted crystals," *J. Am. Ceram. Soc.*, **83**, [1], 214-16 (2000).